PNAS RESEARCH ARTICLE | NEUROSCIENCE OPEN ACCESS

Transformation of acoustic information to sensory decision variables in the parietal cortex

Justin D. Yao[a,b,c,1,2], Klavdia O. Zemlianova[a,1,2], David L. Hocker[a], Cristina Savin[a,d,e], Christine M. Constantinople[a,d], SueYeon Chung[a,f], and Dan H. Sanes[a,d,g,h]

Edited by Yang Dan, University of California, Berkeley, CA; received July 15, 2022; accepted November 8, 2022

The process by which sensory evidence contributes to perceptual choices requires an understanding of its transformation into decision variables. Here, we address this issue by evaluating the neural representation of acoustic information in the auditory cortex-recipient parietal cortex, while gerbils either performed a two-alternative forced-choice auditory discrimination task or while they passively listened to identical acoustic stimuli. During task engagement, stimulus identity decoding performance from simultaneously recorded parietal neurons significantly correlated with psychometric sensitivity. In contrast, decoding performance during passive listening was significantly reduced. Principal component and geometric analyses revealed the emergence of low-dimensional encoding of linearly separable manifolds with respect to stimulus identity and decision, but only during task engagement. These findings confirm that the parietal cortex mediates a transition of acoustic representations into decision-related variables. Finally, using a clustering analysis, we identified three functionally distinct subpopulations of neurons that each encoded task-relevant information during separate temporal segments of a trial. Taken together, our findings demonstrate how parietal cortex neurons integrate and transform encoded auditory information to guide sound-driven perceptual decisions.

parietal cortex | auditory perception | decision-making | neural response manifold | geometric analysis

Significance

Consider walking along a busy street and suddenly hearing heavy footsteps approaching behind you. Deciding whether to move aside to avoid an impending collision becomes more evident with the sound of each additional footstep. This process requires integrating sensory observations over time and is implemented by transforming stimulus representations into decision variables. We explored the underlying neural mechanisms by recording parietal cortex activity while animals either performed an auditory task or passively listened to the identical sounds. While behaviorally relevant auditory information is represented when animals listen passively to the stimuli, it is only during task engagement that decoded parietal cortex activity directly reflects psychometric performance and behavioral measures of integration time.

Integrating sensory information over time is one of the fundamental attributes that is required for accurate perceptual decisions (1, 2). This process is supported by the transformation of stimulus representations into decision variables. In the case of auditory stimuli, prior to the formation of decision variables, the central representations of acoustic cues are gradually reconfigured along the auditory neuraxis. Thus, auditory neurons become more selective to contextually relevant acoustic features as one ascends the central pathway into the auditory cortex (3). Ultimately, individual acoustic components merge into auditory objects to guide perception (4). Similarly, primary visual cortex neurons are selective to the stimulus orientation (5, 6), whereas higher cortices are selective for more complex characteristics (7–9). A hierarchical progression of sensory information processing is also seen across the somatosensory ascending pathway where receptive fields grow more complex (10). These hierarchically transformed neural signals are ultimately decoded downstream of sensory cortices for stimulus-dependent decisions (4, 11–14).

Studies in both nonhuman primates and rodents suggest that the parietal cortex integrates sensory inputs and transforms them into decision signals (15–19). The parietal cortex receives direct projections from primary or secondary sensory cortices (20, 21), has been causally implicated in the performance of perceptual decision-making tasks (22–25), and its activity typically reflects action selection (26, 27). Furthermore, parietal neurons gradually increase their spiking activity over time epochs that scale with the accumulation of sensory evidence (11, 28–31). Thus, while parietal cortex activity reflects decision variables, the manner in which relevant sensory stimuli are represented prior to this transformation remains uncertain.

To dissociate encoding of stimuli from encoding of decision, we recorded neural activity from the parietal cortex while gerbils performed an auditory discrimination task (25), and again during passive listening sessions, using the same acoustic stimuli in the absence of behavioral decision. While some visual studies have explored visual selectivity of parietal cortex neurons under passive fixation conditions (32, 33), a direct comparison between the decoding of visual stimuli versus decision would require that eye fixation be controlled during stimulus presentation. In contrast, auditory tasks can be performed without the need to maintain head position during a trial, permitting us to directly compare the sound-driven responses of parietal cortex neurons during task engagement versus their responses to identical stimuli during passive listening. Thus, we predicted that if parietal cortex activity during task performance did not reflect the transition into decision-related

Author contributions: J.D.Y. and D.H.S. designed research; J.D.Y. performed research; J.D.Y., K.O.Z., D.L.H., C.S., C.M.C., and S.Y.C. contributed new reagents/analytic tools; J.D.Y., K.O.Z., and D.L.H. analyzed data; and J.D.Y., K.O.Z., D.L.H., and D.H.S. wrote the paper.

The authors declare no competing interest.

This article is a PNAS Direct Submission.

[1]J.D.Y. and K.O.Z. contributed equally to this work.

[2]To whom correspondence may be addressed. Email: justin.yao@rutgers.edu or koz200@nyu.edu.

This article contains supporting information online at https://www.pnas.org/lookup/suppl/doi:10.1073/pnas.2212120120/-/DCSupplemental.

Published January 4, 2023.

variables, then all analyses of neural processing would be similar to those displayed during the passive listening condition. We found that during task performance, decoded parietal cortex population activity based on stimulus identity correlated with behavioral discrimination across similar timescales. Furthermore, principal component analysis (PCA) performed on parietal cortex responses revealed neural trajectories (i.e., the change in parietal cortex population activity over time) that demonstrated the temporal progression of low-dimensional encoding of acoustic information that transitioned to encoding of behavioral choices. During passive listening sessions, decoding performance from parietal cortex population activity based on stimulus identity was poorer than decoding during task performance, but scaled with stimulus duration. In addition, the PCA revealed neural trajectories that differentiated between each stimulus condition, but did not reflect a decision variable. Thus, the parietal cortex could accumulate auditory evidence for the purpose of forming a decision variable during task performance. Finally, our clustering analysis based on neuronal response properties suggest subpopulations of parietal neurons that may reflect separate temporal segments of individual trials during decision-making. We propose that the parietal cortex integrates and transforms bottom-up sensory information into decision variables during task performance.

Results

We trained gerbils (n = 5) to perform a single-interval, two-alternative forced-choice (AFC) amplitude modulation (AM) rate discrimination task (25). Gerbils were trained to self-initiate each trial by placing their nose in a cylindrical port for 100 ms. On each trial, a 4- or 10-Hz AM signal was presented from an overhead speaker and animals approached the left or right food tray on the opposite side of the test cage. A food pellet reward was delivered when animals approached the left food tray following a 4-Hz AM signal or the right food tray following a 10-Hz AM signal (Fig. 1*A*). To measure the minimum time necessary to accurately perform the task, AM stimulus duration was varied across trials (100 to 2,000 ms), and performance was quantified as the proportion of correct trials. Fig. 1*B* shows example psychometric functions from two different animals. In both examples, task performance improved with increasing stimulus duration and reached an optimum at ≥800 ms. *SI Appendix*, Fig. S1 displays psychometric functions for all five gerbils (n = 44 sessions). Minimum integration time was defined as the shortest stimulus duration at which animals discriminated between the two AM signals at a performance level of 0.76, which is equivalent to the signal detection metric, *d'* of 1 (34). The distribution of minimum integration times across all sessions is shown at the bottom of *SI Appendix*, Fig. S1. There was no significant difference between minimum integration times for the 4- and 10-Hz AM signals (Wilcoxon signed-rank test, $P = 0.67$; 4-Hz minimum integration time median: 391 m; 10-Hz minimum integration time median: 402 ms), demonstrating animals were not biased in preferentially approaching the left or right food tray that were linked to the corresponding stimuli.

To assess parietal cortex neuron responses during task performance, we implanted trained animals with 64 channel electrode arrays, and obtained wireless recordings during auditory discrimination task performance. These recordings were compared with the neural responses recorded while animals listened passively to the identical acoustic stimuli (Fig. 1*C*). Recorded physiological data (Fig. 1*D*) were preprocessed to extract candidate waveforms for offline spike sorting procedures. One anatomically confirmed electrode track within the parietal cortex is shown in Fig. 1*E*. We recorded a total of 297 units (22.9%, 68/297 classified as single-units) during task performance sessions and 284 units during passive listening sessions (22.9%, 65/284 classified as single-units). *SI Appendix*, Fig. S2 shows example poststimulus time histograms (PSTHs) for one unit during one task performance and one passive listening session. The responses of all recorded units to long (2,000 ms) and short (300 ms) stimulus durations are shown in Fig. 1 *F* and *G*. Although there was a diversity of PSTH patterns during task performance, a fraction of parietal units displayed an initial decline in spike rate, followed by a gradual increase during the AM target stimuli. This temporal pattern of neural response was similar to that observed by parietal neurons during visual decision-making that also displayed ramping activity with increasing sensory evidence (29, 35, 36). In contrast, a differential firing rate across time was less robust during passive listening sessions.

To determine whether parietal cortex population activity was sufficient to account for sound-driven task performance, we constructed linear classifiers using support vector machines (SVM) (37) (see *Methods*). Briefly, AM discrimination was quantified across our parietal cortex population with a linear population readout scheme. Spike count responses from recorded neurons were counted within 100-ms time windows across the entire trial durations. This temporal bin size did not change as the analysis time window expanded across stimulus durations. The population linear classifiers were trained to decode responses from a proportion of trials to each individual AM rate signal (4- versus 10-Hz) across each stimulus duration (Fig. 2*A*). Cross-validated classification performance was determined as the proportion of correctly classified held-out trials. Thus, decoding performance represents the discriminability of stimulus identity (4- versus 10-Hz AM rate). This population decoder analysis was applied to our dataset in two ways. First, decoder performance was assessed from simultaneously recorded single- and multiunits within each behavioral session (i.e., "within-session" analysis; Fig. 2*B*). Second, we assessed decoder performance for all units pooled across all behavioral sessions (Fig. 2*F*).

For the within-session analysis, we implemented a standard criterion to only assess sessions with a minimum of five simultaneously recorded single- and/or multiunits (n = 31/44 sessions). Fig. 2*B* shows example within-session population decoder results from two animals during task performance. In both cases, decoding performance increases with longer stimulus durations, in line with psychometric performance. Decoding performance and corresponding behavioral performance for each stimulus type (4- and 10-Hz AM rate) across all sessions are shown in *SI Appendix*, Fig. S3*A*. Neural minimum integration times were calculated as the stimulus duration corresponding to decoding performance of 0.76. The distributions of neural minimum integration times are plotted in *SI Appendix*, Fig. S3*B*. We found a significant positive correlation between behavior integration times and corresponding decoder integration times (Fig. 2*C*; r = 0.49, $P = 0.02$), and similar trends were observed for both trial types (*SI Appendix*, Fig. S3*C*; 4-Hz AM: r = 0.54, $P = 0.01$; 10-Hz AM: r = 0.44, $P = 0.05$). This suggests parietal cortex activity reflects auditory-based decisions.

We next asked whether the time course of decoder performance aligned with behavioral integration times. Fig. 2*D* displays average ± SEM decoding performance as a function of time for correct left (4-Hz) versus right (10-Hz) trials across all 31 recorded sessions. Since we were interested in the time points of decoding performance, this analysis was based on a 100-ms sliding window. At trial onset, decoding performance was near chance, and then increased to a peak value of ~0.80 (average ± SEM, left: 0.81 ± 0.03; right: 0.80 ± 0.03).

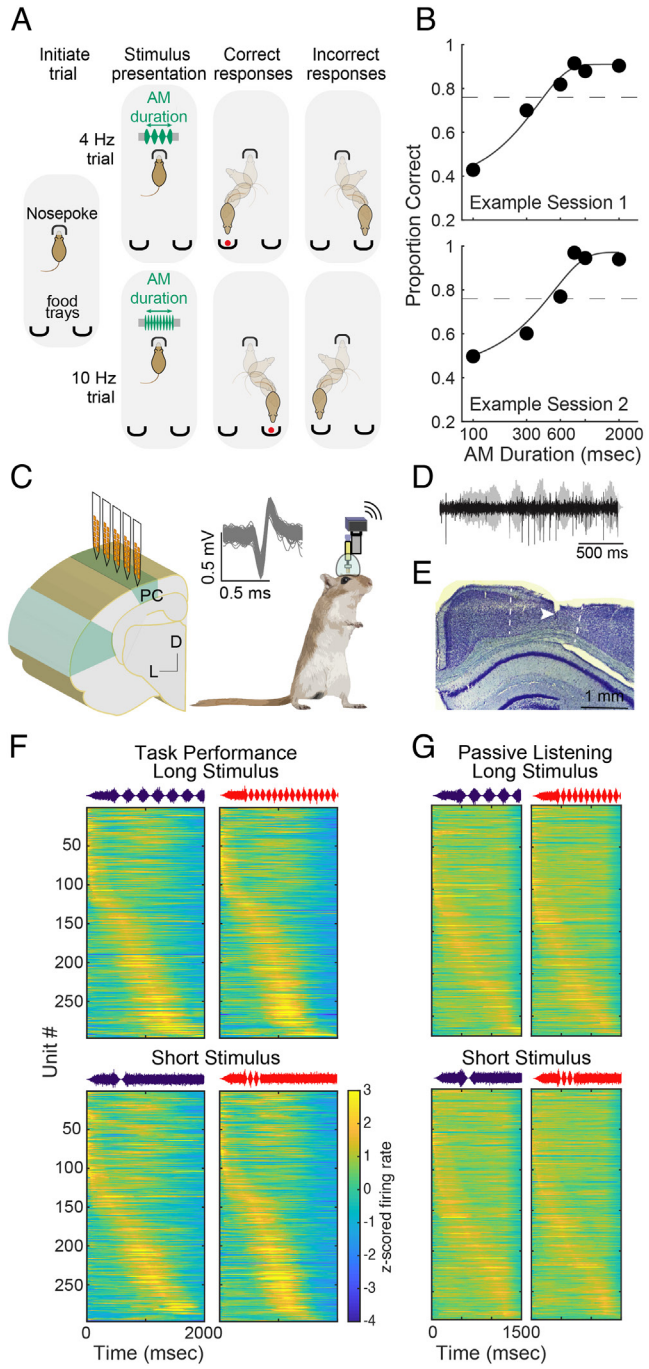

Fig. 1. Behavioral measures of auditory task performance and neural recordings. (*A*) Schematic of the single-interval, two-AFC AM rate discrimination task. Gerbils are required to discriminate between AM broadband noise presented at 4- versus 10-Hz across a range of stimulus durations (100 to 2,000 ms). (*B*) Two example psychometric functions from two animals. (*C*) Chronic 64-channel electrode arrays were implanted into the left parietal cortex of five gerbils. (*D*) Raw waveform trace of neural response to AM signal. (*E*) Anatomically confirmed electrode track within the parietal cortex. (*F*) Z-scored firing rate activity of all parietal cortex neurons during task performance sessions (n = 297) for "Long Stimulus" duration of 2,000 ms (*Top*) and "Short Stimulus" duration of 300 ms (*Bottom*), sorted by time of maximum firing rate. (*G*) Same format as panel *F*. Z-scored firing rate activity of parietal cortex neurons during the passive listening session (n = 284), sorted by time of maximum firing rate. Note that the total stimulus time is shorter for passive listening because trials did not exceed a total stimulus time of 1,500 ms.

The maximum decoding performance occurred at ~350 ms of AM signal duration, which is nearly identical to the average behavioral integration time (378 ms; *SI Appendix*, Fig. S1). Decoding performance decreases after this time point, suggesting that the animals no longer temporally integrate the sensory information and may begin to initiate their motor approach toward the corresponding food tray. To further illustrate decision-related activity across trial durations, we also plotted decoding performance as a function of time relative to response latency (*SI Appendix*, Fig. S3*D*). Decoding performance gradually begins to increase ~1,000 ms prior to response latency and decoding performance peaks ~600 ms prior to response latency.

Although the striking alignment of neural and behavioral performance suggests that auditory information is being integrated within the parietal cortex, it does not provide a direct measure of stimulus coding. Therefore, we recorded from the same parietal neurons studied during task performance while animals listened passively to the identical 4- and 10-Hz AM stimuli (Fig. 1*G* and *SI Appendix*, Fig. S2*B*). Within-session population decoder results for two passive listening sessions are shown in Fig. 2*E*. Decoding performance across all sessions for each stimulus type is shown in *SI Appendix*, Fig. S3*E*. The distributions of neural minimum integration times during passive listening sessions are plotted in *SI Appendix*, Fig. S3*F*. Overall, only a fraction of passive listening sessions yielded minimum integration times (n = 17/29; maximum decoding performance did not reach 0.76 for the remaining 12 sessions). For these passive listening sessions, decoding performance scaled with increasing stimulus duration (Fig. 2*E* and *SI Appendix*, Fig. S3*E*), suggesting that the parietal cortex could accumulate this sensory evidence for the purpose of forming a decision variable.

To directly compare decoder performance during task performance and passive listening, we examined the 19 instances where corresponding session types fit the criterion of five simultaneously recorded units. In the majority of those instances (13/19 sessions), integration time was better or could only be calculated during task performance (*SI Appendix*, Fig. S3*G*). In six cases, integration time diminished or could not be calculated during task performance (*SI Appendix*, Fig. S3*H*). Neurometric function slopes were similar between task performance versus passive listening sessions ($P = 0.47$; Wilcoxon signed rank test).

We further examined decoding performance as a function of the number of total recorded units for task performance and passive listening sessions (Fig. 2*F*). A subsampling procedure was applied to randomly select a subpopulation of units (25 to 297 for task performance and 25 to 284 for passive listening sessions; increasing increments of 25) across 500 iterations. During each iteration of the resampling procedure, a new subpopulation of units was randomly selected (without replacement) prior to the decoding readout procedure. For each stimulus duration, decoding performance for both task performance and passive listening session types increased with the number of units, demonstrating evidence for population-level encoding.

Given that we could decode both stimulus identity, and the behavioral integration times from the neural activity, we predicted that the parietal cortex would transform the sensory inputs into low-dimensional decision variables. Low-dimensional decision variables are beneficial from the computational point of view as they would permit a downstream decoder to efficiently read out the decision, and use the information to implement a corresponding motor action plan. Thus, we predicted that population activity would gradually diverge into two independent patterns that corresponded to the two sound-driven decision categories (e.g., 4-Hz: choose left and 10-Hz: choose right). To test this idea, we assessed the dynamics of parietal cortex population activity by applying PCA to the trial-averaged neural responses (Fig. 3*A*). This analysis was conducted on two of the five recorded animals as they both provided the large majority of recorded units (Gerbil 1 n =

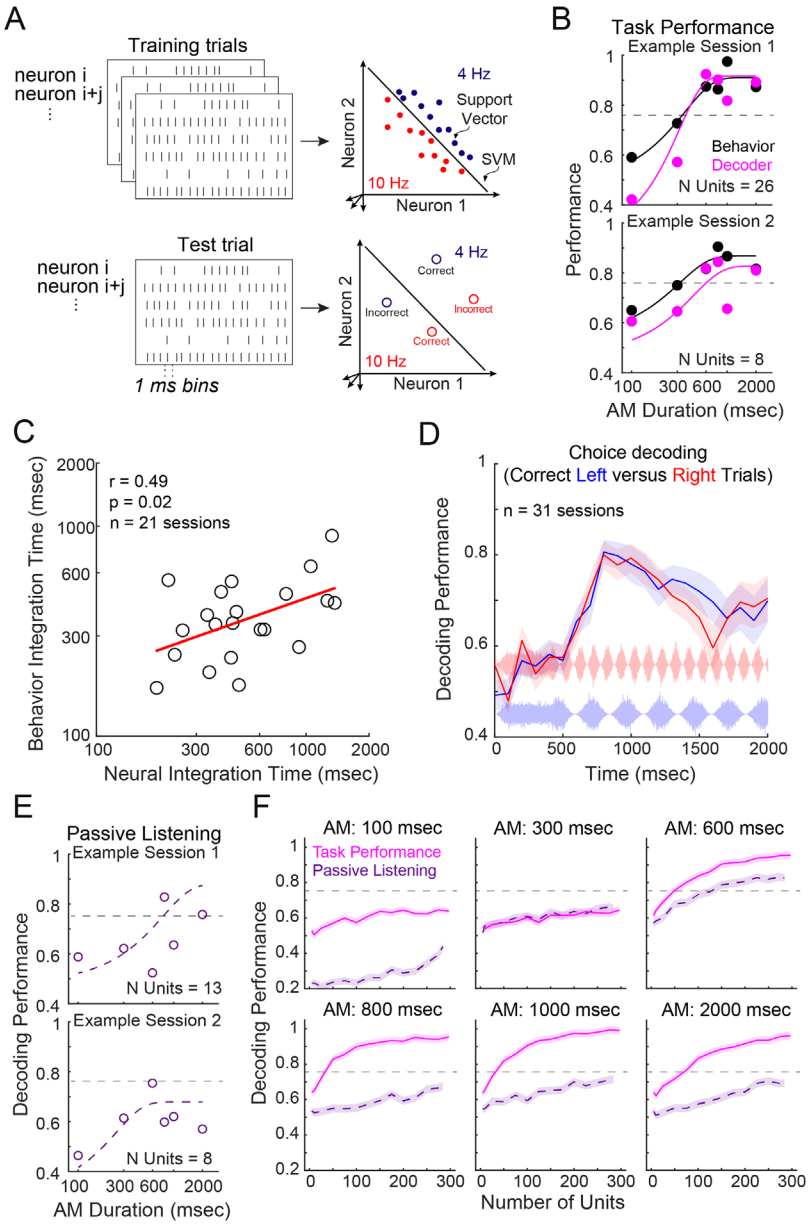

Fig. 2. Parietal cortex population activity reflects auditory task performance and contains auditory information. (*A*) Schematic of linear population readout procedure. Population linear classifiers were trained to decode the responses from a subpopulation of simultaneously recorded parietal cortex neurons from a proportion of trials to each AM rate signal (4 Hz versus 10 Hz) across each stimulus duration. Cross-validated classification performance was determined as the proportion of correctly classified held-out trials that were not used during classifier training. This procedure was performed across 250 iterations with new randomly drawn sampled train and held-out trials for each iteration. (*B*) Within-session population decoder results (pink) and corresponding behavior performance (black) from two example sessions from two animals during task performance. Dashed horizontal lines are plotted at 0.76 proportion of correct trials. Minimum integration time was defined as the stimulus duration at which proportion of correct trials = 0.76, which is equivalent to $d' = 1$ (see *Methods*). (*C*) Corresponding behavior versus neural integration times from the same sessions. For each session, behavioral integration time is taken from the psychometric function (e.g., Fig. 2*B*, black curves), and neural integration time is taken from the neurometric function (e.g., Fig. 2*B*, pink curves). Measurements of corresponding behavior and neural integration times could only be measured from 21 sessions. For other instances, psychometric and/or neural decoding performance did not reach the criterion of 0.76, and an integration time could not be measured. Solid red line represents the linear regression. Pearson's r and statistical significance are noted in the *Top-Left* corner of the figure panel. (*D*) Average ± SE within-session decoding performance for correct left versus right trials from all sessions (n = 31) that fit the criterion of five simultaneously recorded single- and/or multi-units. (*E*) Within-session population decoder results from two example sessions from two animals during passive listening sessions. (*F*) Population decoding performance for task performance (pink) and passive listening (purple) conditions across increasing number of recorded units for each stimulus condition. A resampling procedure was used to randomly select a subpopulation of units with increasing increments of 25 across 500 iterations prior to applying the decoding readout procedure. Decoding performance for both session types increased with the number of units. For all stimulus durations except 300 ms, decoding performance during task performance exceeded that of passive listening sessions across all unit totals. For passive listening sessions, maximum decoding performance was found when including all recorded units, whereas decoding performance during task performance reached its peak when including ~≥80% of total units. Maximum decoding performance for task performance sessions asymptotes higher than passive listening sessions, but are comparable between 300 and 600 ms stimulus duration (*SI Appendix*, Fig. S3*I*), which is near the average behavioral integration time. Error bars denote average ± SEM.

115/297 units; Gerbil 2 n = 165/297 units). Fig. 3*B* depicts population activity in a three-dimensional (3D) principal component space that originated from PSTHs of recorded units from two animals during task performance (top three principal components, explained variance: Gerbil 1 = 79.7%; Gerbil 2 = 88.8%). The neural trajectories in this state space correspond to the population responses across different times for each AM rate and the stimulus durations. At stimulus onset, neural trajectories started at a similar position, but began to diverge toward the relevant decision, or stimulus identity, subspace (4-Hz versus 10-Hz) after ~300 ms of acoustic stimulation in support of our prediction. This divergence toward the relevant decision subspace over time is further demonstrated when we measured the Euclidean distance between each pair of trajectories in the space spanned by the top three principal components (*SI Appendix*, Fig. S4*A*). Over time, the distance between the trajectories that correspond to the stimulus durations of opposing AM rates (4-Hz versus 10-Hz) dramatically increased (*SI Appendix*, Fig. S4*A*, *Upper Right* and *Lower Left Quadrants* of each matrix; outlined in red), while the average distance between the trajectories that correspond to the stimulus durations within each AM rate remained low (*SI Appendix*, Fig. S4*A*, *Upper Left* and *Lower Right Quadrants* of each matrix). In other words, the resulting distance matrix is block diagonal showing that trajectories corresponding to the same stimulus identity remained closer to each other than to the trajectories corresponding to the opposite stimulus identity – thereby indicating the existence of decision-relevant manifolds. We define "manifold" as the collection of population neural responses that encode a stimulus. This block diagonal structure further demonstrates that these manifolds are independent of stimulus features that are irrelevant to the decision, such as stimulus duration. PCA performed on the pooled dataset yielded very similar results (*SI Appendix*, Fig. S5). Together, these results suggest the formation of low-dimensional decision-relevant manifolds and are consistent with the integration of sensory evidence over time and the representation of a decision variable by the neural population. This low-dimensional encoding in manifolds did not necessarily have to be the case. The null hypothesis was that the parietal cortex maintains high dimensional representations from which decisions could be still decoded, but the information would not be organized along a decision category structure.

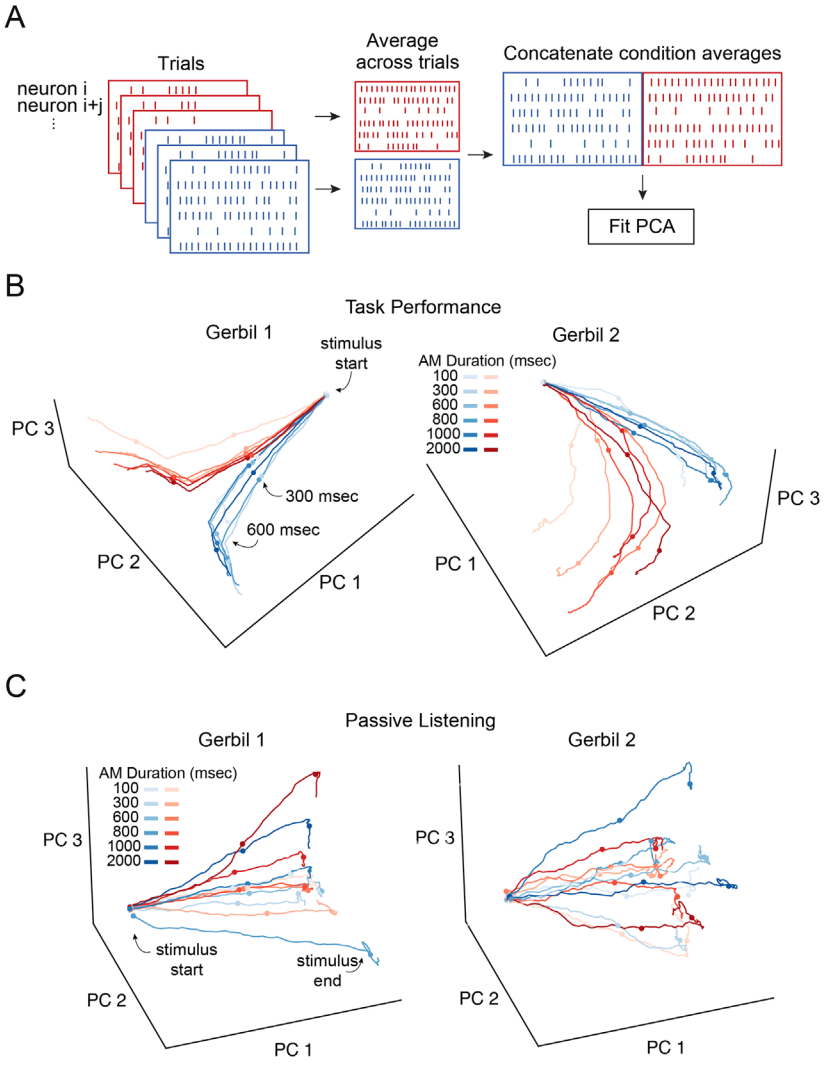

Fig. 3. Parietal cortex population dynamics during task performance. (*A*) PCA was performed on trial averaged neural responses from two of the five implanted gerbils. (*B*) Population activity plotted in a 3D principal component space that originated from PSTHs of all recorded units for two gerbils during task performance. The neural trajectories in this state space correspond to the population responses across different times for separate AM rates and stimulus durations. Dot symbols represent 0, 300, and 600 ms after stimulus (AM) onset. (*C*) Same as (*B*) except during passive listening.

In this case, we would have seen intermingled neural trajectories that were not separated into the two sound-driven decision categories in a low-dimensional projection.

In principle, decision variables should not be computed when animals are disengaged from a sensory task. To test this idea, we performed the same PCA to trial-averaged neural responses recorded during passive listening sessions. Fig. 3*C* depicts population activity in 3D principal component space that originated from PSTHs of recorded units from two animals during passive listening (top three principal components, explained variance: Gerbil 1 = 82.3%; Gerbil 2 = 85.2%). In contrast to the neural trajectories of parietal cortex neural responses during task performance, the neural trajectories elicited during passive listening did not diverge according to the two separate manifolds corresponding to AM rates (*SI Appendix*, Figs. S4*A* versus *SI Appendix*, Figs. S4 *B* and S5 *B*, outlined red squares). This is reflected in the difference in decoding performance between the two behavioral conditions (Fig. 2 *B*, *E*, and *F*). Instead, the neural trajectories elicited by each combination of the AM rate and stimulus duration eventually occupied separate positions in the principal component space. This is further demonstrated by the differences in Euclidean distances between each stimulus condition (*SI Appendix*, Figs. S4 *B* and S5 *B*). Combined with the finding that several passive listening sessions yielded an integration time (n = 17/29; *SI Appendix*, Fig. S3*F*), this suggests that, while acoustic information is encoded in the parietal cortex during passive listening, decision-related variables that are linked with behavioral integration times are not computed.

Previous studies have hypothesized that the brain transforms sensory information into linearly separable representations (38, 39). This "untangling" of representations has been suggested to be a more prominent feature of higher order brain areas (38, 40). Thus, the segregation of neural trajectories from parietal cortex activity into two separate subspaces during task performance may represent an encoding strategy that enables linear readout of decision variables (*SI Appendix*, Fig. S6*A*). To test whether the neural representations of the AM rate stimuli in principal component space are consistent with this prediction, we employed three measures of untangling: capacity, manifold radius, and manifold dimensionality (41). These three measures define the separability of objects based on their neural manifolds. Capacity measures how many different object classes can be linearly separated with high probability. Manifold radius and dimensionality quantify the size of the manifold; essentially, the variance of the points that belong to the manifold as well as its spread along different axes. To compute these measures, we first binned the spiking activity into 80-ms bins and then split the trial activity into two conditions according to the AM rates, 4- and 10-Hz, combining across stimulus durations as well as all of the animals. Consistent with the concept of untangling, we found that there was an increase in capacity

(*SI Appendix*, Fig. S6*B*) and a decrease in manifold radius and dimensionality after the onset of the AM stimulus (*SI Appendix*, Fig. S6 *C* and *D*). Finally, we computed the norm of the manifold center over time, which measures the distance of the center of the manifold to the origin, to understand if the object manifolds corresponding to each stimulus identity move over time. This measure gradually increased (*SI Appendix*, Fig. S6*E*), suggesting that the 4- and 10-Hz manifolds moved away from their starting position over time. These trends continue through ~600 ms into the AM stimulus (~1,000 ms of absolute trial time) at which point all four measures plateau. Importantly, the time course of this change in neural representation is consistent with the time window over which the animal has to accumulate evidence and make its decision. Together, our findings suggest that the transformation of sensory evidence into decision variables in the parietal cortex is accompanied by changes in the neural representation that supports the separability of the stimulus manifolds.

The previous analysis of population-level encoding of auditory stimuli and the decision variable assumed that the recorded population was homogeneous. Since the parietal cortex appears to encode both the auditory stimulus, and the decision variable, we predicted that this would occur in functionally distinct subpopulations of neurons. Thus, to determine how these variables are encoded in the parietal cortex, we utilized a complementary set of analysis tools to ask whether their responses are found in distinct functional classes and, if so, whether they differentially represented the emergence of the decision variable. To test this, we performed clustering on PSTHs (42–44). Specifically, for each neuron we averaged over trials with the same AM stimulus rate (4- or 10-Hz) to obtain two conditional PSTHs spanning the 2 s after trial initiation. We then concatenated these 2 PSTHs to create a high-dimensional feature space that represents the unique activity of each neuron across the two stimulus conditions. Analysis of the angles between these data points in feature space tested for significantly smaller angles than would occur in unclustered, gaussian-distributed features (PAIRS test) (42), which indicated that there were clusters in this dataset. We then performed k-means clustering on these responses, with the number of clusters chosen using the gap statistic that determines the statistically significant number of clusters compared to unclustered, gaussian-distributed features. The gap statistic revealed three subpopulations of neurons in the population response (Fig. 4 *A*–*D*). Cluster 1 (n = 163), the largest cluster in the population, demonstrated activity at the onset of unmodulated noise (i.e., the 400 ms before the AM stimulus), and persisted through the trial (Fig. 4 *A* and *B*). Clusters 2 (n = 61) and 3 (n = 73) displayed decreased activity at the beginning of a trial, with a ramping of activity peaking at ~1 s. Clusters 1 and 3 were well-represented, though cluster 2 was predominantly represented in only one gerbil. We confirmed that this clustering result is robust to different forms of preprocessing of the responses, such as downsampling to coarse time bins, or smoothing over multiple time bins (*SI Appendix*, Fig. S7 *A*–*D*). Clustering on the passive condition reveals the presence of two clusters, though the population predominantly belonged to only a single cluster (*SI Appendix*, Fig. S8).

To evaluate the computational roles of each neural cluster and determine whether specific subpopulations of neurons reflect the integration of sensory evidence and the formation of decision variables, we performed PCA on each cluster individually. Specifically, the PCA was fit to trial averaged neural responses across time for the three clusters separately for two of the five gerbils. The neural trajectories in this state space correspond to the population responses for each cluster across different times for separate AM rates and stimulus durations. We show the neural trajectories for each cluster in the space spanned by the top three principal components of each respective cluster (Fig. 4 *E*–*G*). The neural trajectories across all clusters show a separation between the two AM rates, but diverge at separate time points. This suggests that each cluster may encode different task-relevant information. For example, the neural trajectories in the principal component space of clusters 1 (Fig. 4*E*) and 2 (Fig. 4*G*) display strong divergence between the corresponding AM rates much sooner than the neural trajectories of cluster 3 (Fig. 4*F*). Specifically, the divergence of neural trajectories for clusters 1 and 2 occurs within 600 ms after stimulus onset, which corresponds to the behaviorally relevant integration times (*SI Appendix*, Fig. S1). This suggests that clusters 1 and 2 may reflect the transformed sensory signals received from the auditory cortex during task performance. The neural trajectories for cluster 3 diverge later than ~600 ms after stimulus onset (≳1,000 ms total trial duration), suggesting that cluster 3 may reflect the motor preparatory signal that is executed during the task. Overall, our results demonstrate that during task performance, the decision variable is broadly represented across the entire population of parietal cortex neurons, but distinct subpopulations of neurons are active during different task epochs: stimulus integration and putative motor preparation or execution.

Discussion

Our central finding is that, during task performance, parietal cortex neurons integrate and transform behaviorally relevant acoustic information to drive sound-driven perceptual choices. Decoded parietal cortex activity based on stimulus identity reflected psychometric sensitivity during task performance and aligned with behavioral measures of integration time. In contrast, decoded neural activity from passive listening sessions was dramatically reduced. We further supported this finding by investigating the underlying neural representations that lead to our decoder performance. By applying principal component and geometric analyses, we found the emergence of decision-relevant, low-dimensional, linearly separable manifolds that reflect behavioral integration time during task performance. Since it was possible, a priori, that neural representations of parietal cortex activity would be similar during task performance and passive listening, this finding confirms that the parietal cortex mediates a transition into decision-related variables. Using a clustering analysis, we then identified three different neural populations that each encoded task-relevant information during different temporal segments of the trial. Taken together with our previous finding that auditory cortex projections to the parietal cortex play a causal role in producing behavioral integration time (25), we propose that the parietal cortex transforms auditory afferent input into low-dimensional decision variables encoded at the neural population level.

Previous work shows that parietal cortex neurons are strongly modulated by the behavioral relevance and context of acoustic stimuli (45–48). Furthermore, functional interactions of simultaneously recorded parietal neurons are greater than that seen among auditory cortex neurons and also extend to longer time scales (18), demonstrating the transition to timescales that match behavioral integration time. These functional properties are clearly associated with anatomical connectivity between primary or secondary auditory cortices to the parietal cortex, which are strongly apparent across many species (21, 25, 49–52).

Our current results complement these findings by demonstrating how auditory encoded information is transformed from an uninformative representation during passive listening, to meaningful integration times that reflect behavioral performance. During passive listening, decoded activity from simultaneously recorded parietal cortex neurons is poorer than decoded activity

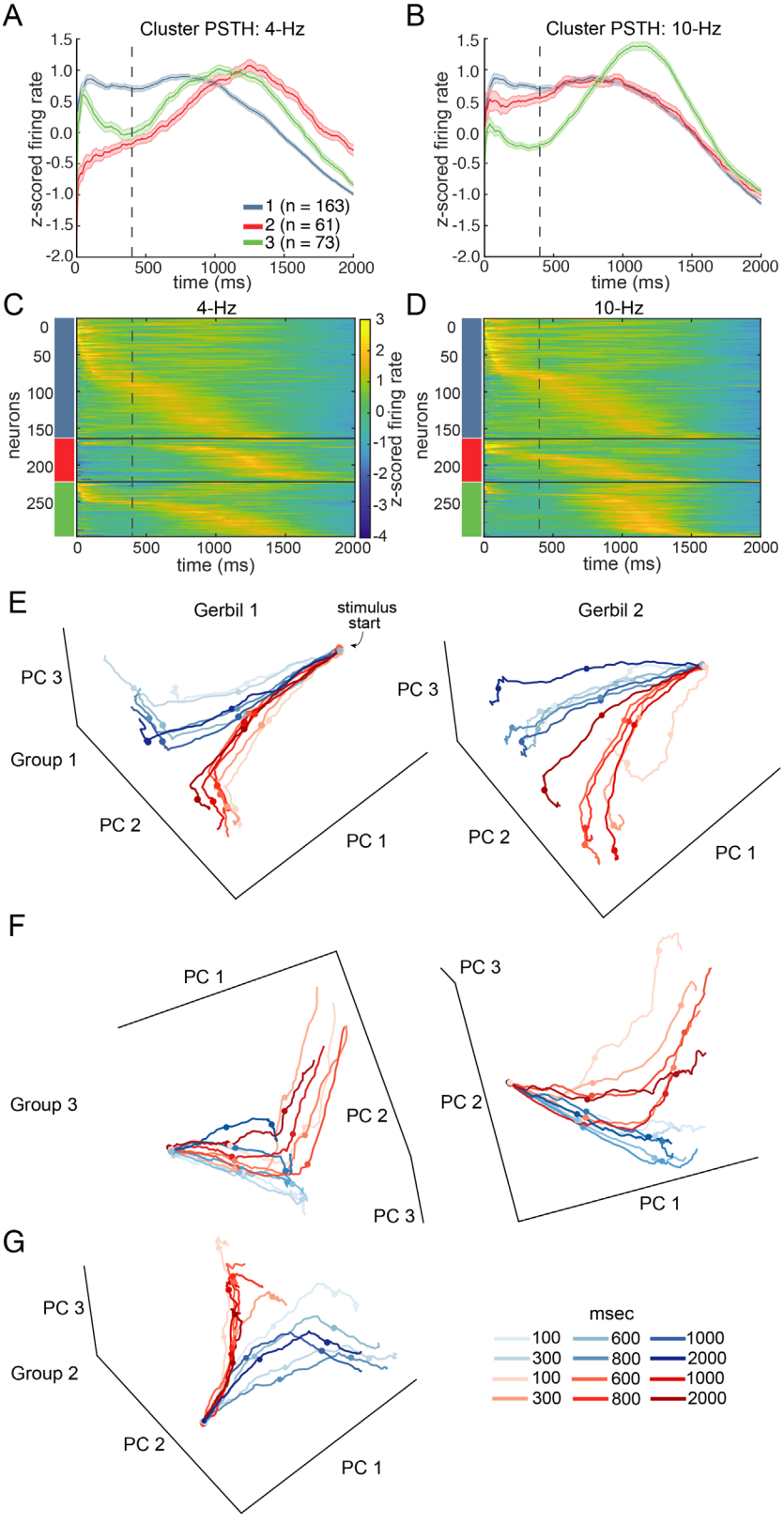

Fig. 4. Clustering of conditional PSTH responses reveals three distinct subpopulations of neurons in the parietal cortex. (*A*) Cluster-averaged PSTH for 4-Hz AM stimulus. Dashed line indicates onset of the 4- and 10-Hz AM stimulus, and error bars denote average ± SE. (*B*) Similar to (*A*) except for 10-Hz AM stimulus. (*C*) Population PSTH responses for 4-Hz AM stimulus. Responses are grouped by cluster identity (colored rectangles), and sorted by time of maximum firing rate within each cluster, for each stimulus condition. (*D*) Similar to (*C*) except for 10-Hz AM stimulus. (*E*) Population activity plotted in a 3D principal component space that originated from PSTHs of "Group 1" units for two gerbils during task performance. Dot symbols represent 0, 300, and 600 ms after stimulus (AM) onset. (*F*) Similar to (*E*) except for "Group 3" units. (*G*) Similar to (*E*) except for "Group 2" units.

during task performance, but scales with stimulus duration (Fig. 2*E*). Thus, evidence for encoded sensory inputs within parietal cortex derives from the scaling of decoded parietal cortex activity with the amount of presented stimulus information. Our principal component analyses further demonstrate an even greater difference of parietal cortex activity between behavioral conditions. While encoded auditory information from parietal neurons occupied separate positions in subspace during passive listening (Fig. 3*C* and *SI Appendix*, Fig. S4*B*), we found an emergence of decision-relevant, linearly separable manifolds during task performance that corresponded to behavioral integration time (Fig. 3*B* and *SI Appendix*, Fig. S4*A*). This is specifically demonstrated by a clear separation of manifolds that correspond to the two AM rates (4- and 10-Hz), which is also reflected by two separate

decision outcomes (e.g., approach the left or right food tray). If parietal cortex activity during task performance did not reflect the transition into decision-related variables, then the neural trajectories would be similar to the passive listening condition. The transition of sensory encoding between passive and task-engaged contexts suggests that sensory information transitions into a decision-making context and reflects the learned association between sensory categorization and motor execution. This is in contrast to categorical sensory representations (53), which would be true if parietal cortex neurons represented stimulus categories during passive listening conditions. Enhanced decision-relevant categorization during task engagement can be found in auditory cortex neurons. For example, ferret auditory cortex neurons display greater decoding performance for behaviorally driven sounds during task performance over passive listening, but only in the post-stimulus silent interval (54). Therefore, it is possible this persistent change in auditory cortex neuronal activity is driven by descending inputs from the parietal cortex. It is worth noting that our recordings for the passive condition were collected from the same highly trained animals, so the differences in representation cannot be explained by the lack of association between stimulus and decision.

Our principal component and geometric analyses demonstrated that decision variables emerge within parietal cortex activity during task performance. We predicted that the role of the parietal cortex is to transform stimulus information into a representation that can be easily decoded into action. While the neural manifolds that correspond to 4- and 10-Hz AM rates increasingly diverge during task performance (Fig. 3*B* and *SI Appendix*, Fig. S5), these representations become more "untangled," or linearly separable, over behaviorally relevant timescales (*SI Appendix*, Fig. S6). This is computationally desirable because it suggests that the parietal cortex can read out auditory information using the simplest possible decoder. This result is consistent with predictions from artificial neural network models for auditory processing (55) and is also consistent with previous findings that individual neurons show mixed selectivity for task variables (36) and may change activity patterns without affecting the overall ability of the population to encode the relevant task information (19). Finally, our result shows that this untangling of representations occurs not only by compression in dimensionality and size of the stimulus manifolds, but also by the stimulus manifolds moving away from each other.

Clustering on the temporal responses of parietal cortex neurons provided finer grained detail of the encoding of the decision variable in the parietal cortex that were characterized with the other analyses. During task performance, clustering revealed three subpopulations of neurons, with two clusters being well represented. One subpopulation ("Cluster 1") demonstrated the encoding of AM stimulus information, while the other dominant subpopulation ("Cluster 3") displayed a gradual increase in activity that peaked much later within a trial, compared with the other two clusters. We interpret this late-in-trial segment is likely related to preparatory movement activity, motor initiation, or movement as the animal approaches one of the two food trays near the end of a trial. A third cluster ("Cluster 2") seemed to share a similar phenotype with cluster 1 since its corresponding neural trajectories diverged relatively around the same time. However, when comparing PSTHs, cluster 2 neuronal responses were more modulated for ipsilateral (left; 4-Hz) conditions, relative to cluster 1. It is important to note that this cluster was only present in one gerbil. It is possible that neurons from cluster 2 may belong to cluster 1, or alternatively, observing ipsilateral encoding of sensory evidence integration is simply a rare type of response property in the parietal cortex.

Previous studies did not find separable clusters when examining the mixed selectivity of parietal cortex activity (42). In that work, PAIRS analysis was performed on time-averaged activity across different sensory stimuli (auditory and visual), and found that responses were not separable into distinct subpopulations. Our results in parietal cortex responses instead used time-dependent response profiles that were restricted to a single stimulus modality to analyze potential clustering. We believe that these two results do not conflict, and that taken together they highlight how clustering is a flexible tool to characterize a variety of encoding properties across subpopulations of neurons. To our knowledge, clustering on temporal responses to identify functional subpopulations has only been documented in the frontal cortex (43, 44, 56). Thus, our results here suggest that the approach may be of more general utility across higher cortical regions in which multiple cognitive variables are encoded.

While our study focused on the sensory input to the parietal cortex, it did not address the neural mechanism that causes the transformation of sensory representations into decision variables. This process is thought to require descending input from the prelimbic region of the frontal cortex (21, 57). The cingulate cortex may provide one source of task-relevant information to the parietal cortex as neurons can encode context-dependent signals, which can be read out by locus coeruleus activity (58). This provides a potential neural circuit for appropriately modulating parietal cortex activity during task performance, where represented encoded sensory information is integrated, grouped, and transformed into decision variables that can be projected to motor circuits (16).

Our results do not indicate whether the formation of sensory-driven decisions also occurs in premotor circuits, such as those that strictly involve action planning, including striatal circuits (59). Furthermore, our results do not demonstrate whether the auditory temporal integration signals observed are exclusively computed within the parietal cortex, or reflect a computation performed elsewhere in the brain that are contingent on motor execution, such as brainstem networks (60–63). Future work will determine whether the transformation of sensory integrated signals into task-engaged decision variables occurs within separate neural circuits and/or is dependent on the execution of motor actions, such as the movements associated to report the decisions (64).

In summary, the representation of behaviorally relevant auditory information occurs in the parietal cortex even when animals are passively listening to the stimuli. However, it is only during task engagement where decoded parietal cortex activity directly reflects psychometric performance and behavioral measures of integration time. Additionally, it is only during task engagement that we find the formation of low-dimensional manifolds that are distinct based on stimulus identity and ultimately, decision. We demonstrated this with principal component and geometric analyses, each of which show that sensory evidence is accumulated across a time frame that matches behavioral integration time (25). Thus, our findings provide a plausible argument for the parietal cortex's role in integrating and transforming encoded auditory information into decision variables to guide sound-driven behavior.

Materials and Methods

Adult Mongolian gerbils (*Meriones unguiculatus*, n = 5, three males) were weaned from commercially obtained breeding pairs (Charles River). Animals were housed on a 12-h light/12-h dark cycle and provided with ad libitum food and water unless otherwise noted. All procedures were approved by the Institutional Animal Care and Use Committee at New York University.

Behavior.

Behavioral apparatus. Adult gerbils were placed in a plastic test cage (0.4 × 0.4 × 0.4 m) in a sound-attenuating booth (GretchKen Industries, Inc; internal dimensions: 1.5 × 1.5 × 2.2 m) and observed via a closed-circuit monitor. Acoustic stimuli were delivered from a calibrated free-field tweeter (DX25TG0504; Vifa) positioned 1 m above the test cage. Sound calibration measurements were made with a 1/4-inch free-field condenser recording microphone (Brüel and Kjaer) placed in the center of the cage. Stimulus, food reward delivery, and behavioral data acquisition were controlled by a personal computer through custom MATLAB scripts (written by Daniel Stolzberg: https://github.com/dstolz/epsych) and an RZ6 multifunction processor (Tucker-Davis Technologies).

Psychophysical training and testing was implemented with a positive reinforcement appetitive one-interval AFC procedure, as described previously (25). Briefly, gerbils were placed on controlled food access and trained to discriminate between amplitude-modulated (AM) frozen broadband noise (25-dB roll-off at 3.5 kHz and 20 kHz) at 4- versus 10-Hz at 100% modulation depth. Each AM stimulus was presented at a sound pressure level (SPL) of 66 dB and had a 200 ms onset ramp, followed by an unmodulated period of 200 ms that transitioned to an AM signal for a set duration, followed by an unmodulated period. Gerbils self-initiated trials by placing their nose in a cylindrical port (nose poke) for a minimum of 100 ms that interrupted an infrared beam and triggered an acoustic stimulus. During acoustic stimulation, a gerbil approaches the left or right food tray and the infrared beam at the correct food tray is broken, a pellet dispenser (Med Associates) delivers one reward dustless precision pellet (20 mg; Bio-Serv). Gerbils were first trained to distinguish between 4- versus 10-Hz AM with a stimulus duration of 2,000 ms (proportion of trials correct >0.85) across two sessions, and then were presented with shorter durations (e.g., 1,000, 800, 600, 300, and 100 ms) across subsequent sessions. For each trial, the probability of a 4- or 10-Hz AM stimulus presentation is 50%, and its duration is a random draw. Fig. 1*A* displays the schematic of the task.

During sessions to assess perceptual sensitivity, six signal durations for each of the 4- and 10-Hz AM stimuli (100, 300, 600, 800, 1,000, and 2,000 ms) are presented. Integration time is assessed by examining how performance scales with stimulus duration. Proportions of correct trials across stimulus durations for each AM rate are fitted with psychometric functions using the open-source package psignifit 4 for MATLAB (65). Psychometric functions of the proportion of correct trials are plotted as a function of stimulus duration. Minimum integration time was defined as the stimulus duration at which proportion of correct trials = 0.76, which is equivalent to the signal detection metric, d', equal to 1 (34).

Electrophysiology. Extracellular single- and multiunit activity was recorded from the left medial parietal cortex. After gerbils were trained in the behavioral task, a silicon probe with 64 recording sites was implanted into the left medial parietal cortex (Neuronexus, model Buszaki64_5x12-H64LP_30mm). We targeted the medial portion of the parietal cortex because of its robust auditory cortex-recipient anterograde labeling (25). The probe was attached to a manual microdrive (Neuronexus, dDrive-XL) that allowed the electrode to be advanced and retracted. Probes were inserted at a 0° to 10° angle on a mediolateral axis. Typically, we aimed the rostral most shanks of the array to be positioned at 3.3 to 3.6 mm rostral and 2.5 mm lateral to lambda. The surgical implantation procedure was performed under isoflurane anesthesia. Animals recovered for at least 1 wk before being placed on controlled food access for further psychometric testing. At the termination of each experiment, animals were deeply anesthetized with sodium pentobarbital (150 mg/kg) and perfused with phosphate-buffered saline and 4% paraformaldehyde. Brains were extracted, postfixed, sectioned on a vibratome (Leica), and stained for Nissl. Brightfield images were inspected under an upright microscope (Revolve Echo) and compared with a gerbil brain atlas (66) to verify the targeted medial parietal cortex.

Physiological data were acquired telemetrically from freely moving animals with a wireless headstage and received (W64, Triangle Biosystems). Analog signals were preamplified and digitized at a 24.414-kHz sampling rate (PZ5, Tucker–Davis Technologies) and fed via fiber optic link to the RZ5 base station (Tucker–Davis Technologies) and PC for storage and postprocessing. Offline, electrophysiological signals underwent a common average referencing procedure (67) and bandpass filtered at 300 to 5,000 Hz. Significant noisy portions of the signal that were induced by extreme head movements were removed by an artifact rejection procedure. An open source spike package (KiloSort) (68) was used to extract and cluster spike waveforms. Manual inspection of spike waveforms was conducted in Phy (69). Well-isolated single units displayed clear separation in principal component space and possessed few refractory period violations (<10%). Units that did not meet these criteria were classified as multiunits. All sorted spiking data were analyzed with custom MATLAB scripts. Recordings were made both during task performance, and during passively listening sessions that occurred after task performance. All passively listening sessions were recorded immediately after each recorded task performance session with the nose poke and food trays removed from the test cage.

Neural Analyses.

Population coding. We used a previously employed linear classifier readout procedure (37) to assess AM rate discrimination across a population of parietal cortex neurons. Specifically, a linear classifier was trained to decode responses from a proportion of trials to each stimulus condition (e.g., 4 versus 10 Hz; Fig. 2*A*). Spike count responses from all recorded neurons were counted within 100-msec time windows across the entire trial durations and formed the population "response vector". Since the number of trials was typically unequal between stimulus conditions, we randomly subsampled (without replacement) a proportion of trials (i.e., 15 trials) from each unit. An SVM procedure was used to fit a linear hyperplane to 80% of the data set ("training set"). Cross-validated classification performance was assessed on the remaining 20% across 250 iterations with a new randomly drawn sampled train and test sets for each iteration. Performance metrics were computed to determine the proportion of correctly classified and misclassified trials using an expanding time window (100-msec increments) across the entire trial duration. We constrained the analysis time window to correspond to each stimulus duration up to 600 msec (e.g., maximum time window did not exceed 300 msec for stimulus duration of 300 msec). A maximum time window of 600 msec was utilized for stimulus durations > 600 msec to control for movement-related signals that may arise when animals approach their selected food tray. This was particularly the case during task performance sessions. The SVM procedure was implemented in MATLAB using the "fitcsvm" and "predict" functions with the "KernelFunction" set to "linear". This analysis was conducted for task sessions with ≥ 5 simultaneously recorded units and performance on easiest trial conditions (e.g., 2,000 ms AM duration) ≥ 85% (n = 27/44 total sessions; median simultaneously recorded units = 6; interquartile range = 6.25).

Population response manifolds. PCA was performed separately for both task performance and passive listening session types for each animal using trial averaged PSTHs. Trial averages were computed by binning the spiking data into 10-ms bins and using a rolling mean with a 50-ms window for each of 12 conditions (2 stimulus AM rates × 6 Durations) with each unit contributing to the PSTH for each condition. The PSTHs focused on the period of decision formation and spanned 400 to 1,400 ms after stimulus onset (0 to 1,000 ms after AM onset). For each unit, we concatenated the PSTH for each condition into a matrix of size N × CT, where C is the number of conditions (2 AM rates × 6 durations), T is the number of time points (10 ms resolution), and N is the number of units. Each row of the matrix was then z-scored, since PCA is known to be sensitive to overly active units. For the task performance condition, only trials where the animal made the correct choice were used in the analysis. Trials with only one spike in the time window of interest were left out from analysis. Units that had no data for one or more of the conditions were left out from the analysis. Finally, the analysis included all units recorded either simultaneously or separately. We confirmed that the same qualitative results (the presence of decision subspace during task performance and lack of one during passive listening) were obtained using simultaneously recorded units only.

Calculating distance between neural trajectories. To calculate the distance between every pair of trial averaged trajectories for each time point (*SI Appendix*, Fig. S4), we computed the Euclidean norm between the same time point for every pair of averaged trajectories in the space defined by the top three principal components.

Geometric Analysis. To understand how the representation of stimulus information in the parietal cortex changes over the course of decision-making, we use the mean-field theoretic manifold analysis technique (38, 41, 55) to study the geometric properties of the stimulus manifolds, including their manifold capacity, radius, and dimensionality. Unlike SVM, these measures consider the geometric structure of the manifold when computing separability. To prepare the data, we counted the number of spikes per neuron in each 80-ms time bin for each correct trial for the

first 1,200 ms of each trial. Next, we define two object manifolds, corresponding to the 4- and 10-Hz stimulus. We subsampled 50 trials, combining across stimulus durations and animals, for each object manifold. Together, this formed a matrix of size (297 neurons × 2 object manifolds × 50 trials × 14 time points). The neural activations for each stimulus frequency over the 50 trials defines the manifold for that stimulus frequency at each time point. The mean-field theoretic manifold analysis technique then uses this set of activations to compute geometric properties of each object manifold and to evaluate their linear separability. Calculation of each measure was performed using the Replica Mean Field Theory Analysis python library (55), but we briefly describe the methodology below.

Manifold capacity refers to the maximum number of object manifolds that can be linearly separable given a fixed number of features. If we consider P object manifolds and N neurons, the manifold capacity is defined as $\alpha = P/N$. Intuitively, when α is small, then there are few manifolds in a high-dimensional space thus making it very easy to find a separating hyperplane for most of the random dichotomy of labels. Alternatively, when α is large, there are many object manifolds in a low-dimensional space and therefore, it becomes less likely that any dichotomy of manifolds can be linearly separable. The critical manifold capacity, as computed in our analysis, refers to the maximum number of object manifolds P that can be linearly separated given N neurons. This quantity can be estimated from the statistics of anchor points, representative support vectors defining the optimal separating hyperplane, following the methods described in ref. 41. In *SI Appendix*, Fig. S6, we report manifold capacity relative to its lower bound of $2/M$, where M is the number of samples.

Manifold dimensionality, computed from the realized anchor points, estimates the embedding dimension of the manifold contributing to classification. The dimensionality is bounded above by $min(M, N)$. Since we have $M < N$, we report manifold dimensionality relative to M in *SI Appendix*, Fig. S6*D*.

Manifold radius is the average distance between the center of the manifold and its anchor points. For linear separability, we care about the size of manifolds relative to how far they are from each other. The manifold radius is therefore reported relative to the norm of the center of the manifold. We also compute the norm of the center of the manifold separately in *SI Appendix*, Fig. S6*E* to estimate how the locations of the manifolds shift over time.

Clustering. Neuronal responses were clustered using K-means on a feature space comprised of trial-averaged, conditional PSTHs for left-cued and right-cued trials. PSTHs were binned into 10-ms bins, and were then smoothed over a 500-ms moving window to reduce noise on the responses (Matlab's smooth.m function). Each PSTH was then z-scored and combined into a total data matrix $Z \in R^{N \times 2T}$, where N is the number of neurons and $T = 151$ is the number of data points for each conditional PSTH. PCA was performed on Z to reduce the dimensionality of population responses to obtain principal components W and score M, as $Z = MW^T$. This feature space required $k = 16$ components to explain >95% of the covariance in Z. The first k columns of M (data projection onto the top principal components) were used as the feature space for clustering.

The gap statistic criterion was used to determine a principled choice of the best number of clusters (evalclusters.m in Matlab, 5,000 samples for reference distribution) (70). Specifically, the chosen cluster was defined as the largest cluster size K, beyond which jumps in gap score Gap(K) plateaued and became insignificant,

$$Gap(K) \geq Gap(K-1) + 2SE(K-1).$$

We used the PAIRS statistic to determine if clusters were present in conditional PSTH responses of parietal neurons (42, 44). The dimensionality reduced feature space (i.e., the first k columns of M) were further preprocessed with a whitening transform to yield zero mean and unit covariance. For each data point, the average angle with $m = 4$ of its closest neighbors, $\tilde{\theta}_{data}$, was calculated. This angle distribution was compared with $N = 10{,}000$ sets of independent draws from a reference Gaussian distribution [$N(0,I)$], with the same number of data points and the same dimensionality as our data. These N datasets were aggregated into a grand distribution, giving the estimated angles $\tilde{\theta}_{ref}$. The number of nearest neighbors m is conventionally chosen as the number of neighbors required to give a median nearest neighbor angle $\pi/4$ for the reference distribution. This number is dependent on the dimensionality of the data, and given the high dimensionality of these responses, even $m = 2$ neighbors yielded larger angles than $\pi/4$. We chose $m = 4$ for the results in this work, but note that significant clustering was seen for a wide range of m values ($m = [2, 6]$).

PAIRS is a summary statistic of these averages nearest neighbor angles, using the median from the data distribution, $\tilde{\theta}_{data}$ and the median of the grand reference distributions $\tilde{\theta}_{ref}$:

$$PAIRS = \frac{\tilde{\theta}_{ref} - \tilde{\theta}_{data}}{\tilde{\theta}_{ref}}.$$

To calculate P-values for the PAIRS statistic, reference $PAIRS$ values were generated for each of the N reference data sets, and the two-sided P value (assuming a normal distribution) for the data PAIRS compared with the distribution of reference PAIRS values were reported. We additionally performed a Kolmogorov–Smirnov test on the grand reference distribution and data distribution of median nearest neighbor angles.

Statistics. Statistical analyses and procedures were implemented with custom-written MATLAB scripts (The Mathworks) that incorporated the MATLAB Statistics Toolbox or in JMP 13.2.0 (SAS). Normally distributed data (as assessed by the Lilliefors test) are reported as mean ± SEM unless otherwise stated. When data were not normally distributed, nonparametric statistical tests were used when appropriate.

Data, Materials, and Software Availability. Data and analysis code can be found at https://nyu.box.com/v/Yao-Zemlianova-et-al-2022 (71). All study data are included in the article and/or *SI Appendix*.

ACKNOWLEDGMENTS. We thank members of the Sanes laboratory for constructive comments and feedback on the analyses and data interpretation. We also thank John Rinzel, Alex Williams, and Amitabha Bose for helpful comments on this study. This work was supported by the National Institute on Deafness and Other Communication Disorders at the National Institute of Health (grant numbers K99DC018600 to J.D.Y.; R01DC011284 to D.H.S.).

Author affiliations: [a]Center for Neural Science, New York University, New York, NY 10003; [b]Department of Otolaryngology, Head and Neck Surgery, Rutgers Robert Wood Johnson Medical School, New Brunswick, NJ 08901; [c]Brain Health Institute, Rutgers University, Piscataway, NJ 08854; [d]Neuroscience Institute, New York University Langone School of Medicine, New York, NY 10016; [e]Center for Data Science, New York University, New York, NY 10011; [f]Flatiron Institute, Simons Foundation, New York, NY 10010; [g]Department of Psychology, New York University, New York, NY 10003; and [h]Department of Biology, New York University, New York, NY 10003

1. C. D. Brody, T. D. Hanks, Neural underpinnings of the evidence accumulator. *Curr. Opin. Neurobiol.* **37**, 149–157 (2016).
2. M. N. Shadlen, R. Kiani, Decision making as a window on cognition. *Neuron* **80**, 791–806 (2013).
3. X. Wang, Cortical coding of auditory features. *Annu. Rev. Neurosci.* **41**, 527–552 (2018).
4. J. K. Bizley, Y. E. Cohen, The what, where and how of auditory-object perception. *Nat. Rev. Neurosci.* **14**, 693–707 (2013).
5. D. H. Hubel, T. N. Wiesel, Receptive fields, binocular interaction and functional architecture in the cat's visual cortex. *J. Physiol.* **160**, 106–154 (1962).
6. D. H. Hubel, T. N. Wiesel, Receptive fields and functional architecture of monkey striate cortex. *J. Physiol.* **195**, 215–243 (1968).
7. N. C. Rust, J. J. Dicarlo, Selectivity and tolerance ("invariance") both increase as visual information propagates from cortical area V4 to IT. *J. Neurosci.* **30**, 12978–12995 (2010).
8. J. J. DiCarlo, D. Zoccolan, N. C. Rust, How does the brain solve visual object recognition. *Neuron* **73**, 415–434 (2012).
9. J. A. Movshon, E. P. Simoncelli, Representation of naturalistic image structure in the primate visual cortex. *Cold Spring Harb. Symp. Quant. Biol.* **79**, 115–122 (2014).
10. Y. Iwamura, Hierarchical somatosensory processing. *Curr. Opin. Neurobiol.* **8**, 522–528 (1998).
11. J. I. Gold, M. N. Shadlen, The neural basis of decision making. *Annu. Rev. Neurosci.* **30**, 535–574 (2007).
12. J. Tsunada, A. S. Liu, J. I. Gold, Y. E. Cohen, Causal contribution of primate auditory cortex to auditory perceptual decision-making. *Nat. Neurosci.* **19**, 135–142 (2016).
13. J. I. Gold, A. A. Stocker, Visual decision-making in an uncertain and dynamic world. *Annu. Rev. Vis. Sci.* **3**, 227–250 (2017).
14. S. M. Town, K. C. Wood, J. K. Bizley, Sound identity is represented robustly in auditory cortex during perceptual constancy. *Nat. Commun.* **9**, 4786 (2018).
15. M. N. Shadlen, W. T. Newsome, Neural basis of a perceptual decision in the parietal cortex (area LIP) of the rhesus monkey. *J. Neurophysiol.* **86**, 1916–1936 (2001).
16. C. D. Harvey, P. Coen, D. W. Tank, Choice-specific sequences in parietal cortex during a virtual-navigation decision task. *Nature* **484**, 62–68 (2012).
17. D. J. Freedman, J. A. Assad, Neuronal mechanisms of visual categorization: An abstract view on decision making. *Annu. Rev. Neurosci.* **39**, 129–147 (2016).
18. C. A. Runyan, E. Piasini, S. Panzeri, C. D. Harvey, Distinct timescales of population coding across cortex. *Nature* **548**, 92–96 (2017).
19. L. N. Driscoll, N. L. Pettit, M. Minderer, S. N. Chettih, C. D. Harvey, Dynamic reorganization of neuronal activity patterns in parietal cortex. *Cell* **170**, 986–999.e16 (2017).

20. T. A. Hackett *et al.*, Feedforward and feedback projections of caudal belt and parabelt areas of auditory cortex: Refining the hierarchical model. *Front. Neurosci.* **8**, 72 (2014).
21. A. A. Wilber *et al.*, Cortical connectivity maps reveal anatomically distinct areas in the parietal cortex of the rat. *Front. Neural Circuits* **8**, 146 (2014).
22. T. D. Hanks, J. Ditterich, M. N. Shadlen, Microstimulation of macaque area LIP affects decision-making in a motion discrimination task. *Nat. Neurosci.* **9**, 682–689 (2006).
23. L. N. Katz, J. L. Yates, J. W. Pillow, A. C. Huk, Dissociated functional significance of decision-related activity in the primate dorsal stream. *Nature* **535**, 285–288 (2016).
24. A. M. Licata *et al.*, Posterior parietal cortex guides visual decisions in rats. *J. Neurosci.* **37**, 4954–4966 (2017).
25. J. D. Yao, J. Gimoto, C. M. Constantinople, D. H. Sanes, Parietal cortex is required for the integration of acoustic evidence. *Curr. Biol.* **30**, 3293–3303.e4 (2020).
26. R. A. Andersen, H. Cui, Intention, action planning, and decision making in parietal-frontal circuits. *Neuron* **63**, 568–583 (2009).
27. E. J. Hwang, J. E. Dahlen, M. Mukundan, T. Komiyama, History-based action selection bias in posterior parietal cortex. *Nat. Commun.* **8**, 1242 (2017).
28. J. D. Roitman, M. N. Shadlen, Response of neurons in the lateral intraparietal area during a combined visual discrimination reaction time task. *J. Neurosci.* **22**, 9475–9489 (2002).
29. R. Kiani, T. D. Hanks, M. N. Shadlen, Bounded integration in parietal cortex underlies decisions even when viewing duration is dictated by the environment. *J. Neurosci.* **28**, 3017–3029 (2008).
30. T. D. Hanks *et al.*, Distinct relationships of parietal and prefrontal cortices to evidence accumulation. *Nature* **520**, 220–223 (2015).
31. Y. Zhou, D. J. Freedman, Posterior parietal cortex plays a causal role in perceptual and categorical decisions. *Science* **365**, 180–185 (2019).
32. A. B. Sereno, J. H. R. Maunsell, Shape selectivity in primate lateral intraparietal cortex. *Nature* **395**, 500–503 (1998).
33. M. C. Romero, P. Pani, P. Janssen, Coding of shape features in the macaque anterior intraparietal area. *J. Neurosci.* **34**, 4006–4021 (2014).
34. M. J. Hacker, R. Ratcliff, A revisted table of d′ for M-alternative forced choice. *Percept. Psychophys.* **26**, 168–170 (1979).
35. A. C. Huk, M. N. Shadlen, Neural activity in macaque parietal cortex reflects temporal integration of visual motion signals during perceptual decision making. *J. Neurosci.* **25**, 10420–10436 (2005).
36. G. Okazawa, C. E. Hatch, A. Mancoo, C. K. Machens, R. Kiani, Representational geometry of perceptual decisions in the monkey parietal cortex. *Cell* **184**, 3748–3761.e18 (2021).
37. J. D. Yao, D. H. Sanes, Developmental deprivation-induced perceptual and cortical processing deficits in awake-behaving animals. *Elife* **7**, e33891 (2018).
38. U. Cohen, S. Chung, D. D. Lee, H. Sompolinsky, Separability and geometry of object manifolds in deep neural networks. *Nat. Commun.* **11**, 746 (2020).
39. S. Chung, L. F. Abbott, Neural population geometry: An approach for understanding biological and artificial neural networks. *Curr. Opin. Neurobiol.* **70**, 137–144 (2021).
40. J. J. DiCarlo, D. D. Cox, Untangling invariant object recognition. *Trends Cognit. Sci.* **11**, 333–341 (2007).
41. S. Chung, D. D. Lee, H. Sompolinsky, Classification and geometry of general perceptual manifolds. *Physical Rev. X* **8**, 031003 (2018).
42. D. Raposo, M. T. Kaufman, A. K. Churchland, A category-free neural population supports evolving demands during decision-making. *Nat. Neurosci.* **17**, 1784–1792 (2014).
43. V. M. K. Namboodiri *et al.*, Single-cell activity tracking reveals that orbitofrontal neurons acquire and maintain a long-term memory to guide behavioral adaptation. *Nat. Neurosci.* **22**, 1110–1121 (2019).
44. D. L. Hocker, C. D. Brody, C. Savin, C. M. Constantinople, Subpopulations of neurons in lOFC encode previous and current rewards at time of choice. *Elife* **10**, e70129 (2021).
45. B. Stricanne, R. A. Andersen, P. Mazzoni, Eye-centered, head-centered, and intermediate coding of remembered sound locations in area LIP. *J. Neurophysiol.* **76**, 2071–2076 (1996).
46. K. Nakamura, Auditory spatial discriminatory and mnemonic neurons in rat posterior parietal cortex. *J. Neurophysiol.* **82**, 2503–2517 (1999).
47. A. Grunewald, J. F. Linden, R. A. Andersen, Responses to auditory stimuli in macaque lateral intraparietal area. I. Effects of training. *J. Neurophysiol.* **82**, 330–342 (1999).
48. J. F. Linden, A. Grunewald, R. A. Andersen, Responses to auditory stimuli in macaque lateral intraparietal area. II. Behavioral modulation. *J. Neurophysiol.* **82**, 343–358 (1999).
49. D. N. Pandya, H. G. Kuypers, Cortico-cortical connections in the rhesus monkey. *Brain Res.* **13**, 13–36 (1969).
50. R. L. Reep, H. C. Chandler, V. King, J. V. Corwin, Rat posterior parietal cortex: Topography of corticocortical and thalamic connections. *Exp. Brain Res.* **100**, 67–84 (1994).
51. J. P. Rauschecker, S. K. Scott, Maps and streams in the auditory cortex: Nonhuman primates illuminate human speech processing. *Nat. Neurosci.* **12**, 718–724 (2009).
52. Y. H. Song *et al.*, A neural circuit for auditory dominance over visual perception. *Neuron* **93**, 1236–1237 (2017).
53. T. Banno, J. H. Lestang, Y. E. Cohen, Computational and neurophysiological principles underlying auditory perceptual decisions. *Curr. Opin. Physiol.* **18**, 20–24 (2020).
54. S. Bagur *et al.*, Go/No-Go task engagement enhances population representation of target stimuli in primary auditory cortex. *Nat. Commun.* **9**, 2529 (2018).
55. C. Stephenson *et al.*,"Untangling in invariant speech recognition" in *Advances in Neural Information Processing Systems*, in *H. Wallach, H. Larochelle, A. Beygelzimer, F. Alché-Buc, E. Fox, R. Carnett, Eds. (Curran Associates, Inc., Red Hook, NY, 2019)*, pp. 14391–14401.
56. J. Hirokawa, A. Vaughan, P. Masset, T. Ott, A. Kepecs, Frontal cortex neuron types categorically encode single decision variables. *Nature* **576**, 446–451 (2019).
57. S. Granon, B. Poucet, Involvement of the rat prefrontal cortex in cognitive functions: A central role for the prelimbic area. *Psychobiology* **28**, 229–237 (2000).
58. S. Joshi, J. I. Gold, Context-dependent relationships between locus coeruleus firing patterns and coordinated neural activity in the anterior cingulate cortex. *Elife* **11**, e63490 (2022).
59. J. Cox, I. B. Witten, Striatal circuits for reward learning and decision-making. *Nat. Rev. Neurosci.* **20**, 482–494 (2019).
60. G. D. Horwitz, W. T. Newsome, Separate signals for target selection and movement specification in the superior colliculus. *Science* **284**, 1158–1161 (1999).
61. G. D. Horwitz, W. T. Newsome, Target selection for saccadic eye movements: Prelude activity in the superior colliculus during a direction-discrimination task. *J. Neurophysiol.* **86**, 2543–2558 (2001).
62. G. D. Horwitz, A. P. Batista, W. T. Newsome, Representation of an abstract perceptual decision in macaque superior colliculus. *J. Neurophysiol.* **91**, 2281–2296 (2004).
63. G. Felsen, Z. F. Mainen, Neural substrates of sensory-guided locomotor decisions in the rat superior colliculus. *Neuron* **60**, 137–148 (2008).
64. D. J. Freedman, J. A. Assad, A proposed common neural mechanism for categorization and perceptual decisions. *Nat. Neurosci.* **14**, 143–146 (2011).
65. H. H. Schütt, S. Harmeling, J. H. Macke, F. A. Wichmann, Painfree and accurate Bayesian estimation of psychometric functions for (potentially) overdispersed data. *Vision Res.* **122**, 105–123 (2016).
66. S. Radtke-Schuller *et al.*, Brain atlas of the Mongolian gerbil (Meriones unguiculatus) in CT/MRI-aided stereotaxic coordinates. *Brain Struct. Funct.* **221**, 1–272 (2016).
67. K. A. Ludwig *et al.*, Using a common average reference to improve cortical neuron recordings from microelectrode arrays. *J. Neurophysiol.* **101**, 1679–1689 (2009).
68. M. Pachitariu, N. A. K. Steinmetz, N. Shabnam, M. Carandini, K. D. Harris, Fast and accurate spike sorting of high-channel count probes with KiloSort. *Adv. Neural Inform. Process. Syst.* **29,** 4455–4463 (2016).
69. C. Rossant *et al.*, Spike sorting for large, dense electrode arrays. *Nat. Neurosci.* **19**, 634–641 (2016).
70. R. Tibshirani, G. Walther, T. Hastie, Estimating the number of clusters in a data set via the gap statistic. *J. R. Stat. Soc. Series B Stat. Methodol.* **63**, 411–423 (2001).
71. J. D. Yao *et al.*, *Transformation* of acoustic information to sensory *decision* variables in the parietal cortex. NYU Box. https://nyu.app.box.com/folder/167571938763?v=Yao-Zemlianova-et-al-2022. Deposited 25 Oct 2022.